AIP | Journal of Applied Physics

Temperature-sensitive photoluminescent CdSe-ZnS polymer composite film for lock-in photothermal characterization

Liwang Liu, Kuo Zhong, Lei Meng, Danny Van Hemelrijck, Ling Wang, and Christ Glorieux

Citation: Journal of Applied Physics **119**, 224902 (2016); doi: 10.1063/1.4953591
View online: http://dx.doi.org/10.1063/1.4953591
View Table of Contents: http://scitation.aip.org/content/aip/journal/jap/119/22?ver=pdfcov
Published by the AIP Publishing

Articles you may be interested in

Photo-stability and time-resolved photoluminescence study of colloidal CdSe/ZnS quantum dots passivated in Al2O3 using atomic layer deposition
J. Appl. Phys. **120**, 083103 (2016); 10.1063/1.4961425

Exploration of CdTe quantum dots as mesoscale pressure sensors via time-resolved shock-compression photoluminescent emission spectroscopy
J. Appl. Phys. **120**, 043107 (2016); 10.1063/1.4959257

Ligand exchange leads to efficient triplet energy transfer to CdSe/ZnS Q-dots in a poly(N-vinylcarbazole) matrix nanocomposite
J. Appl. Phys. **113**, 083507 (2013); 10.1063/1.4793266

Nonvolatile electrical bistability and operating mechanism of memory devices based on CdSe/ZnS nanoparticle/polymer hybrid composites
Appl. Phys. Lett. **93**, 021913 (2008); 10.1063/1.2959786

Cathodoluminescence and photoluminescence of highly luminescent CdSe/ZnS quantum dot composites
Appl. Phys. Lett. **70**, 2132 (1997); 10.1063/1.119043

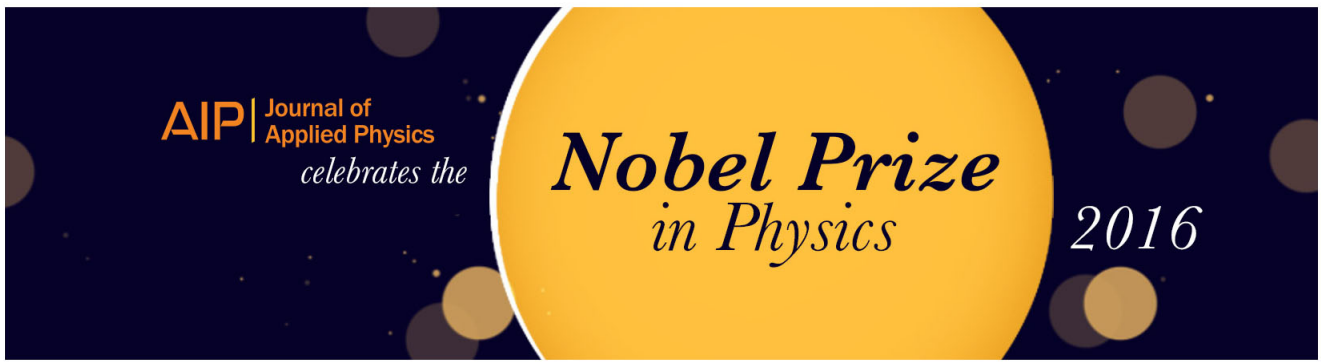

Reuse of AIP Publishing content is subject to the terms at: https://publishing.aip.org/authors/rights-and-permissions. Download to IP: 134.58.253.30 On: Mon, 24 Oct 2016 12:54:18

Temperature-sensitive photoluminescent CdSe-ZnS polymer composite film for lock-in photothermal characterization

Liwang Liu,[1,a)] Kuo Zhong,[2] Lei Meng,[1] Danny Van Hemelrijck,[3] Ling Wang,[1] and Christ Glorieux[1]
[1]*Department of Physics and Astronomy, Laboratory for Soft Matter and Biophysics, KU Leuven, Celestijnenlaan 200D, B-3001 Heverlee, Belgium*
[2]*Department of Chemistry, Molecular Imaging and Photonics, KU Leuven, Celestijnenlaan 200 F- box 2404, 3001 Heverlee, Belgium*
[3]*Department of Mechanics of Materials and Constructions, Vrije Universiteit Brussel, Pleinlaan 2, B-1050 Brussels, Belgium*

(Received 30 March 2016; accepted 27 May 2016; published online 10 June 2016)

The temperature dependence of the fluorescence spectrum of CdSe−ZnS core–shell quantum dots embedded in a polystyrene matrix is characterized between 30 °C and 60 °C. The spectrally integrated photoluminescence intensity is found to linearly decrease with −1.3%/°C. This feature is exploited in a dual coating-substrate-configuration, consisting of a layer of this nanocomposite material, acting as a temperature sensor with optical readout, on top of an optically absorbing and opaque layer, acting as a photothermal excitation source, and covering a substrate material or structure of interest. From the frequency dependence of the optically detected photothermal signal in the frequency range between 5 Hz and 150 Hz, different thermal parameters of the constituent layers are determined. The fitted values of thermal properties of the different layers, determined in different scenarios in terms of the used *a priori* information about the layers, are found to be internally consistent, and consistent with literature values. *Published by AIP Publishing.*
[http://dx.doi.org/10.1063/1.4953591]

I. INTRODUCTION

Quantum dots (QDs) are tiny nanocrystals made of semiconducting material, with diameter in the range of 2–10 nm. Their exceptional photostability, large luminescence quantum yield, and, in particular, the unique size-based tunability of their electronic and optical properties make them very attractive for a wide variety of emerging technologies and applications, e.g., light-emitting diodes (LEDs),[1,2] displays,[3,4] photovoltaics,[5,6] biological labels,[7,8] and optical sensing.[7,9] Previous work has shown that the spectroscopic characteristics for both an ensemble of QDs[10,11] and individual QD[12,13] shift with temperature, thus enabling their use for remote, optical temperature readout through changes in their spectral characteristics. Most often the integrated photoluminescence (PL) intensity has been utilized to extract the temperature, due to the forthright measurement and relatively low cost involved. Since the PL intensity can be affected by mechanical, electrical, and optical instabilities of the measurement arrangement, it can be advantageous to extract the temperature[14–17] from lifetime, spectral shape, ratio-thermometric approaches. The concept of utilizing QDs as optical thermometers has been demonstrated both in near and far field optical configurations. Near field configurations rely on the spatial-controlled scanning of a single QD over the sample surface to be thermally imaged. This is usually accomplished by modifying the tip of an atomic force microscopy (AFM) with QDs.[14,18] Far-field configurations[12,19,20] often involve the direct injection of the QDs into the system of interesting in advance and afterward a superimposition of a fluorescence image of QDs and an optical transmission image, from which thermal imaging can be recovered on the basis of a beforehand calibration of PL features and temperatures. In both cases, however, most of the research has focused on static temperature measurements, rarely on dynamic temperature detection. Recently, we have reported on an ultrafast fluorescence based thermometry in stroboscopic configuration that has a bandwidth up to 100 Mz by means of Rhodamine B as optical probe.[21] In virtue of the similar underlying photochemistry, excellent dynamic performance can be expected as well for QDs based temperature probes, determined by the PL lifetime, which is of the order of tens of nanoseconds at ambient conditions.[22,23] This fast response to temperature changes is advantageous for photothermal detection. Generally, as the temperature is increased, the PL emission of QDs decreases. This can be attributed to thermally assisted energy transfer processes from bulk to surface (non-radiative) states, as well to the escalated interaction between exciton and longitudinal optical (LO) phonon at higher temperatures, leading to enhanced nonradiative decay.[10,22,24] In different types of QDs, such as CdSe,[12] CdSe/ZnS,[11,25] CdTe,[26] and CdTe/ZnS QDs,[27] a notable feature of thermally induced PL quenching is its quasi linear temperature response near ambient temperature (∼20–50 °C). This is again of particular interest for application in photothermal detection, since it provides a constant thermal sensitivity in a typical range of working temperature.

[a)]Author to whom correspondence should be addressed. Electronic mail: liwang.liu@hotmail.com

Reuse of AIP Publishing content is subject to the terms at: https://publishing.aip.org/authors/rights-and-permissions. Download to IP: 134.58.253.30 On: Mon, 24 Oct 2016 12:54:18

In this work, the linear and fast response of the PL integration intensity to temperature is utilized in a photothermal measurement configuration that makes use of an optically absorbing layer and a photoluminescent film, which, combined and illuminated, allow for simultaneous generation and detection of thermal waves.[28,29] The proposed photothermal transducer was fabricated by spin coating a CdSe/ZnS core/shell QD filled polystyrene (PS) composite layer, acting as fast temperature sensing layer, on the top of an optically opaque and absorbing black paint layer, acting as heater (when illuminated). The substrate was a copper slab of 2 mm thickness.

In Section II, we report on the temperature dependence of the PL properties of a spin-coated QDs-PS composite layer on a copper substrate, with a layer of black paint in between serving as absorber layer. The observed linear temperature response is thereafter exploited in a lock-in scheme to monitor PL-detected photothermally induced temperature oscillations between 5 Hz and 150 Hz. In Section III, a 1D multilayer thermal wave model based on the thermal quadrupole approach[30] is elaborated. The thermal properties and thickness of substrate layers are fitted from the experimental data in Section IV. The fits are performed in different scenarios in terms of used *a priori* information on the layer properties, allowing cross-validation. The values are also compared with literature. Conclusions and perspectives for future applications of the approach are given in Section V.

II. TEMPERATURE DEPENDENT PHOTOLUMINESCENCE OF QDS-PS COMPOSITE

CdSe/ZnS core/shell QDs, purchased from Sigma-Aldrich (Lumidot™ CdSe/ZnS), were incorporated in a polystyrene (PS) matrix, by spin-coating (Spin coater Model P6700) at 1000 rpm for 1 min a blend of QD powder (2 mg ml^{-1}) in PS (0.8 g ml^{-1}) toluene onto a polished and cleaned copper substrate of thickness 2 mm. Polystyrene ($M_w \sim 35\,000$), toluene (99%) were all used as purchased from Sigma-Aldrich without further purification. Prior to spin-coating, the copper was coated a layer of black paint (matt black), serving as an optically absorbing layer in the photothermal application. The thicknesses of the QDs-PS layer and black absorber layer, measured by a micrometer (Digimicro, Nikon®), were found to be 13.1 μm and 27.3 μm, respectively.

The temperature dependence of the fluorescence spectrum was determined by means of the setup in Fig. 1 (left). A CW 532-nm laser (Samba 100, Cobolt®) beam was focused with a spot diameter at the sample surface of approximately 20 μm, by an 10×-objective lens (OBL, NA = 0.25), thus exciting the PL of the QDs-PS layer. The emitted PL light was collected by the same OBL and focused by a lens ($F = 10$ mm) onto the fiber entrance of a USB 4000 spectrometer (Ocean Optics®), which recorded the spectrum. The sample was mounted on a hotplate (RET, control-visc, IKA®), with temperature control accuracy of 0.1 K. The temperature control and spectrum acquisition were programmed by a home-made Labview (National Instruments®) program via an RS232 and USB interface, respectively. A typical fluorescence image of the QDs-PS film, taken at room temperature, is presented in Fig. 1 (right).

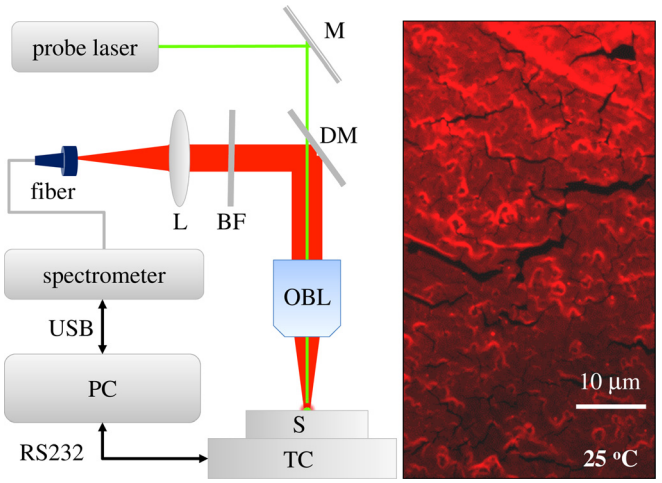

FIG. 1. Experimental setup (left) for measuring the temperature dependent PL of QDs-PS film, and (right) a fluorescence image of the composite taken at 25 °C. M: mirror; DM: dichroic mirror; L: lens, BF: bandpass filter; OBL: objective lens, S: sample, TC: temperature controller.

The cracks were caused by shrinking during drying of the film.[31] The steady-state PL spectrum of the CdSe/ZnS QDs-PS composite film was measured at several selected temperatures, between 30 °C and 60 °C, in steps of 3 °C, as reported in Fig. 2.

The QD spectra are all characterized by a quasi-Gaussian emission shape. The photoluminescence can be attributed to the band-edge recombination of electron–hole pairs within the CdSe core of the QDs.[32] The bandwidth is narrow, approximately 30 nm (0.1 eV) at half maximum. The PL emission is strongly dependent on temperature.[22] The shift of the emission maximum, which is characteristic for the average bandgap of the QDs, evolves monotonically towards longer wavelengths with increasing temperature, as a consequence of energy bandgap shrinkage at higher temperatures,[33] which can be quantified through Varshni[34] equation

$$E_g(T) = E_0 - \frac{AT^2}{T + B}, \tag{1}$$

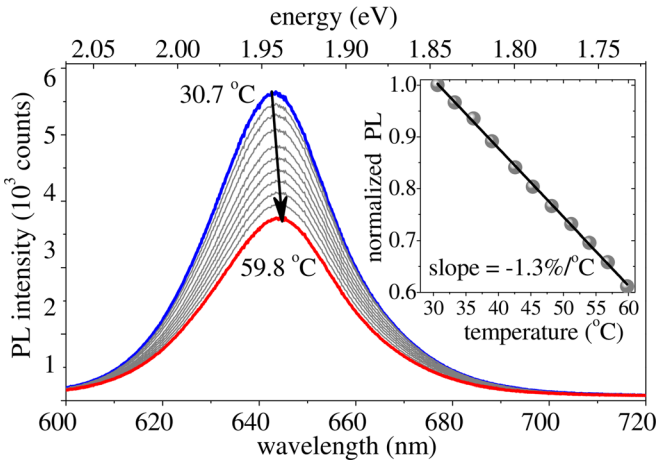

FIG. 2. PL spectra measured at different temperatures, and temperature response of PL intensity (triangles, inset) fitted by a linear function (solid line, inset).

Reuse of AIP Publishing content is subject to the terms at: https://publishing.aip.org/authors/rights-and-permissions. Download to IP: 134.58.253.30 On: Mon, 24 Oct 2016 12:54:18

where E_0 is the band gap energy at 0 K, A is the temperature coefficient, and B is close to the Debye temperature of a material, typically around 150–180 K (Ref. 33) for bulk CdSe. The Varshni relation suggests a quadratic low temperature asymptotic behavior while linear dependence at high temperatures. The observed redshift over a temperature range of 30 K is nearly 3 nm, corresponding to 8.5 meV of bandgap widening, which corresponds to a temperature dependent bandgap change of 2.8×10^{-4} eV K^{-1}. This is consistent with literature values for bulk CdSe $(2.8–4.1) \times 10^{-4}$ eV K^{-1}.[22,24,35] The full width at half maximum (FWHM) of PL emission also broadens slightly as temperature increases, from 30 nm (90 meV) at 30 °C to 31.3 nm (94 meV) at 60 °C. The broadening is due to increased exciton scattering by acoustic and LO phonons.[22] Clearly, the most pronounced spectral change occurs in the PL intensity, which is reduced by 40% throughout the investigated temperature range (inset, Fig. 2). Interestingly, the PL intensity decreases quasi linearly over the range from 30 to 60 °C, by approximately −1.3%/K, in agreement with observations in previous work.[11,12] The linear response to temperature changes of the PL intensity of the CdSe/ZnS QDs over a wide temperature range give them an excellent potential to be used as an optical temperature probe. This is of particular interest for applications in photothermal spectroscopy, which generally involves the detection of photothermally induced heating in time domain (pulsed heating) or frequency domain (modulated heating).

III. LOCK-IN DETECTION OF PHOTOTHERMAL PHOTOLUMINESCENCE SIGNALS

In this section, taking advantage of the rather strong and linear dependence of the fluorescence intensity on temperature, we present the use of the QDs-PS film in a photothermal application. The concept is illustrated in a lock-in detection scheme involving the detection of frequency dependent PL-indicated temperature oscillations. The experimental setup for performing lock-in photothermal PL spectroscopy is depicted in Fig. 3 (left). An 808-nm pump laser (FAP 800, Coherent®) beam, of which the power was sinusoidally modulated by an external function generator (3320 A, Agilent®) at frequency f, was expanded, collimated, and uniformly impinging on the sample surface with a spot size of 8 mm, in order to guarantee 1D heat propagation, at an incident power of 500 mW.

Due to the energy conversion of partially absorbed laser radiation (with intensity variations I(t)) into heat, mainly at the surface of the black paint layer, a thermal wave $\Delta T(t)$ is generated, which in turn modulates the PL intensity, $\Delta I_{PL}(t)$. At the center of the pump beam, where the probe beam was located, as illustrated in Fig. 3 (right), the PL intensity variations were detected by an avalanche photodiode (APD130A, Thorlabs®). The voltage signal produced by the APD was first amplified (SR560, Stanford research systems®) and then fed into a digital lock-in amplifier (SR830, Stanford research systems), by which the amplitude (A_{PL}) and the phase ($\Delta\phi_{PL}$) of the modulated PL signal were determined. In our previous work, this was carried out using offline FFT analysis of the temperature evolution, which was reconstructed from the recorded fluorescence spectrum in the time domain.[15,16] However, the bandwidth in a CW pump-CW probe configuration was limited to 5 Hz by the sampling rate of the spectrometer and by the signal to noise decay with frequency due to the $1/\omega$ dependence of photothermally induced temperature modulation signal. By making use of the following relations (as illustrated in Fig. 4) between the PL intensity oscillations and the underlying temperature oscillations

$$\Delta T \propto -\Delta I_{PL} = -A_{PL} e^{i\Delta\phi_{PL}}, \tag{2}$$

$$\begin{cases} A_T \propto A_{PL} \\ \Delta\phi_T = \Delta\phi_{PL} - \pi, \end{cases} \tag{3}$$

the amplitude (A_T) and phase ($\Delta\phi_T$) signal of the photothermal induced thermal wave can be reconstructed. Note that the negative sign in the right term in Eq. (2) is responsible for the inverse-linear response of the PL to temperature as discussed in Sec. II, which also implies a-π phase delay between the PL intensity oscillation and the temperature oscillation.

The configuration of interest can be described by a 1-D thermal wave diffusion model consisting of three layers (thickness of l_i, $i = 1, 2, 3$), QDs-PS layer, absorber layer, and substrate layer, from top to bottom, respectively, is considered with respect to the actual sample structure and geometry illustrated in Fig. 3 (right). Assuming harmonic modulation of the pump laser intensity (I), the thermal wave

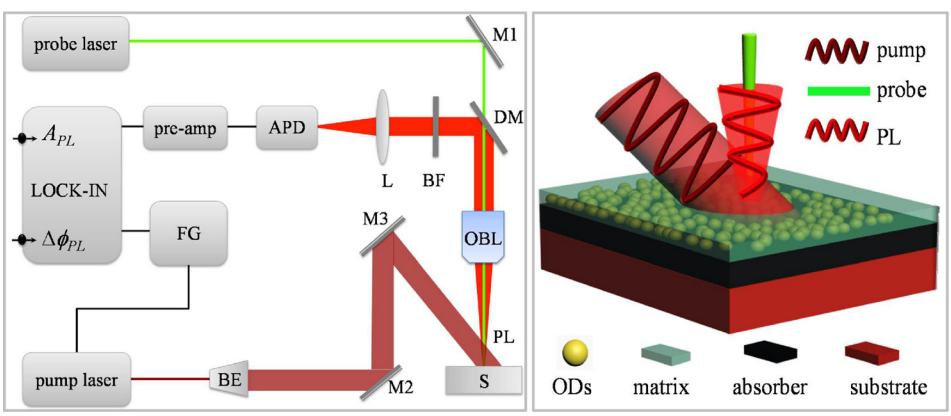

FIG. 3. Experimental setup (left) for lock-in photothermal PL spectroscopy in frequency domain, and light beam configuration (right), with the probe beam located at the center of the pump beam on the surface of the absorber layer (z1). M: mirror; DM: dichroic mirror; L: lens, BF: bandpass filter; OBL: objective lens; S: sample; BE: beam expander; APD: avalanche photodiode.

Reuse of AIP Publishing content is subject to the terms at: https://publishing.aip.org/authors/rights-and-permissions. Download to IP: 134.58.253.30 On: Mon, 24 Oct 2016 12:54:18

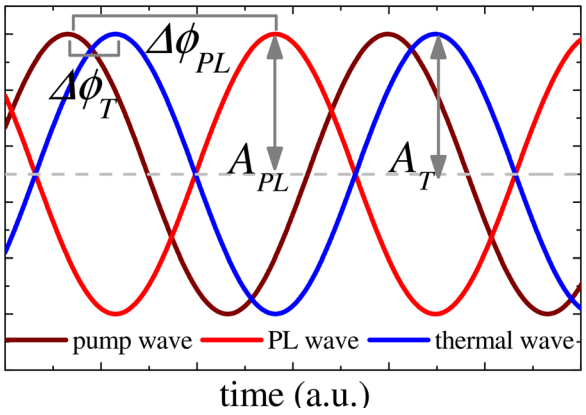

FIG. 4. Illustration of the −180° phase delay between the PL (red) and thermal wave (blue) induced by the modulated pump laser (wine) heating.

equation in the frequency domain (f) at layer i can be written as

$$\frac{\partial^2\Theta_i}{\partial z^2} - {\sigma_i}^2\Theta_i = 0 \tag{4}$$

where $\sigma_i = (j\omega/\alpha_i)^{1/2}$ is the complex thermal wave number ($\omega = 2\pi f$) and α_i is the thermal diffusivity of each layer. The general solution of Eq. (4) can be expressed as

$$\Theta_i(z) = E_i e^{-\sigma_i z} + F_i e^{\sigma_i z}. \tag{5a}$$

For each layer, the heat flux is written by

$$\Phi_i(z) = -\kappa_i \frac{d\Theta_i}{dz} = \kappa_i\sigma_i E_i e^{-\sigma_i z} - \kappa_i\sigma_i F_i e^{\sigma_i z}, \tag{5b}$$

with κ_i is the thermal conductivity of layer i. Below, matrices are given at front and rear surface of each layer:

- Layer 1 (QDs-PS layer)

$$\begin{bmatrix}\Theta_1\\ \Phi_1\end{bmatrix}_{z=0} = \begin{bmatrix}1 & 1\\ \kappa_1\sigma_1 & -\kappa_1\sigma_1\end{bmatrix}\begin{bmatrix}E_1\\ F_1\end{bmatrix}, \tag{6a}$$

$$\begin{bmatrix}\Theta_1\\ \Phi_1\end{bmatrix}_{z=z_1} = \begin{bmatrix}e^{-\sigma_1 z_1} & e^{\sigma_1 z_1}\\ \kappa_1\sigma_1 e^{-\sigma_1 z_1} & -\kappa_1\sigma_1 e^{\sigma_1 z_1}\end{bmatrix}\begin{bmatrix}E_1\\ F_1\end{bmatrix}. \tag{6b}$$

- Layer 2 (absorber layer)

$$\begin{bmatrix}\Theta_2\\ \Phi_2\end{bmatrix}_{z=z_1} = \begin{bmatrix}e^{-\sigma_2 z_1} & e^{\sigma_2 z_1}\\ \kappa_2\sigma_2 e^{-\sigma_2 z_1} & -\kappa_2\sigma_2 e^{\sigma_2 z_1}\end{bmatrix}\begin{bmatrix}E_2\\ F_2\end{bmatrix}, \tag{7a}$$

$$\begin{bmatrix}\Theta_2\\ \Phi_2\end{bmatrix}_{z=z_2} = \begin{bmatrix}e^{-\sigma_2 z_2} & e^{\sigma_2 z_2}\\ \kappa_2\sigma_2 e^{-\sigma_2 z_2} & -\kappa_2\sigma_2 e^{\sigma_2 z_2}\end{bmatrix}\begin{bmatrix}E_2\\ F_2\end{bmatrix}. \tag{7b}$$

- Layer 3 (substrate layer)

$$\begin{bmatrix}\Theta_3\\ \Phi_3\end{bmatrix}_{z=z_2} = \begin{bmatrix}e^{-\sigma_3 z_2} & e^{\sigma_3 z_2}\\ \kappa_3\sigma_3 e^{-\sigma_3 z_2} & -\kappa_3\sigma_2 e^{\sigma_3 z_2}\end{bmatrix}\begin{bmatrix}E_3\\ F_3\end{bmatrix}, \tag{8a}$$

$$\begin{bmatrix}\Theta_3\\ \Phi_3\end{bmatrix}_{z=z_3} = \begin{bmatrix}e^{-\sigma_3 z_3} & e^{\sigma_3 z_3}\\ \kappa_3\sigma_3 e^{-\sigma_3 z_3} & -\kappa_3\sigma_2 e^{\sigma_3 z_3}\end{bmatrix}\begin{bmatrix}E_3\\ F_3\end{bmatrix}. \tag{8b}$$

Thereby a transfer matrix for each layer between the front surface and the rear surface is obtained

$$\begin{bmatrix}\Theta_1\\ \Phi_1\end{bmatrix}_{z=0} = M_1\begin{bmatrix}\Theta_1\\ \Phi_1\end{bmatrix}_{z=z_1}, \tag{9}$$

with

$$M_1 = \begin{bmatrix}1 & 1\\ \kappa_1\sigma_1 & -\kappa_1\sigma_1\end{bmatrix}\begin{bmatrix}e^{-\sigma_1 z_1} & e^{\sigma_1 z_1}\\ \kappa_1\sigma_1 e^{-\sigma_1 z_1} & -\kappa_1\sigma_1 e^{\sigma_1 z_1}\end{bmatrix}^{-1} = \begin{bmatrix}\cosh(\sigma_1 l_1) & \dfrac{\sinh(\sigma_1 l_1)}{\kappa_1\sigma_1}\\ \kappa_1\sigma_1\sinh(\sigma_1 l_1) & \cosh(\sigma_1 l_1)\end{bmatrix},$$

$$\begin{bmatrix}\Theta_2\\ \Phi_2\end{bmatrix}_{z=z_1} = M_2\begin{bmatrix}\Theta_2\\ \Phi_2\end{bmatrix}_{z=z_2}, \tag{10}$$

with

$$M_2 = \begin{bmatrix}e^{-\sigma_2 z_1} & e^{\sigma_2 z_1}\\ \kappa_2\sigma_2 e^{-\sigma_2 z_1} & -\kappa_2\sigma_2 e^{\sigma_2 z_1}\end{bmatrix}\begin{bmatrix}e^{-\sigma_2 z_2} & e^{\sigma_2 z_2}\\ \kappa_2\sigma_2 e^{-\sigma_2 z_2} & -\kappa_2\sigma_2 e^{\sigma_2 z_2}\end{bmatrix}^{-1} = \begin{bmatrix}\cosh(\sigma_2 l_2) & \dfrac{\sinh(\sigma_2 l_2)}{\kappa_2\sigma_2}\\ \kappa_2\sigma_2\sinh(\sigma_2 l_2) & \cosh(\sigma_2 l_2)\end{bmatrix},$$

$$\begin{bmatrix}\Theta_3\\ \Phi_3\end{bmatrix}_{z=z_2} = M_3\begin{bmatrix}\Theta_3\\ \Phi_3\end{bmatrix}_{z=z_3}, \tag{11}$$

with

$$M_3 = \begin{bmatrix}e^{-\sigma_3 z_2} & e^{\sigma_3 z_2}\\ \kappa_3\sigma_3 e^{-\sigma_3 z_2} & -\kappa_3\sigma_2 e^{\sigma_3 z_2}\end{bmatrix}\begin{bmatrix}e^{-\sigma_3 z_3} & e^{\sigma_3 z_3}\\ \kappa_3\sigma_3 e^{-\sigma_3 z_3} & -\kappa_3\sigma_2 e^{\sigma_3 z_3}\end{bmatrix}^{-1} = \begin{bmatrix}\cosh(\sigma_3 l_3) & \dfrac{\sinh(\sigma_3 l_3)}{\kappa_3\sigma_3}\\ \kappa_3\sigma_3\sinh(\sigma_3 l_3) & \cosh(\sigma_3 l_3)\end{bmatrix}.$$

The above derivation suggests the heat transfer matrix can eventually be governed by hyperbolic functions, as explored in thermal quadrupole method.[30] We assume (i) perfect thermal contact between each layer, i.e., continuity of temperature and flux at interfaces, it holds that

$$\begin{bmatrix}\Theta_1\\ \Phi_1\end{bmatrix}_{z=z_1} = \begin{bmatrix}\Theta_2\\ \Phi_2\end{bmatrix}_{z=z_1} - \begin{bmatrix}0\\ Q\end{bmatrix}, \tag{12}$$

$$\begin{bmatrix}\Theta_2\\ \Phi_2\end{bmatrix}_{z=z_2} = \begin{bmatrix}\Theta_3\\ \Phi_3\end{bmatrix}_{z=z_2}. \tag{13}$$

In Eq. (12), Q represents the internal heat source induced by the pump laser, and it should be noted that the internal heat source occurs only at the front surface ($z = z_1$) of the absorber layer, since the top QDs-PS layer is optically transparent for the pump laser while the absorber layer is optically opaque. It is thus easy to obtain $Q = I/2$, and

$$\begin{bmatrix}\Theta_1\\ \Phi_1\end{bmatrix}_{z=0} = \begin{bmatrix}A & B\\ C & D\end{bmatrix}\begin{bmatrix}\Theta_3\\ \Phi_3\end{bmatrix}_{z=z_3} - \begin{bmatrix}a & b\\ c & d\end{bmatrix}\begin{bmatrix}0\\ I/2\end{bmatrix}, \tag{14}$$

Reuse of AIP Publishing content is subject to the terms at: https://publishing.aip.org/authors/rights-and-permissions. Download to IP: 134.58.253.30 On: Mon, 24 Oct 2016 12:54:18

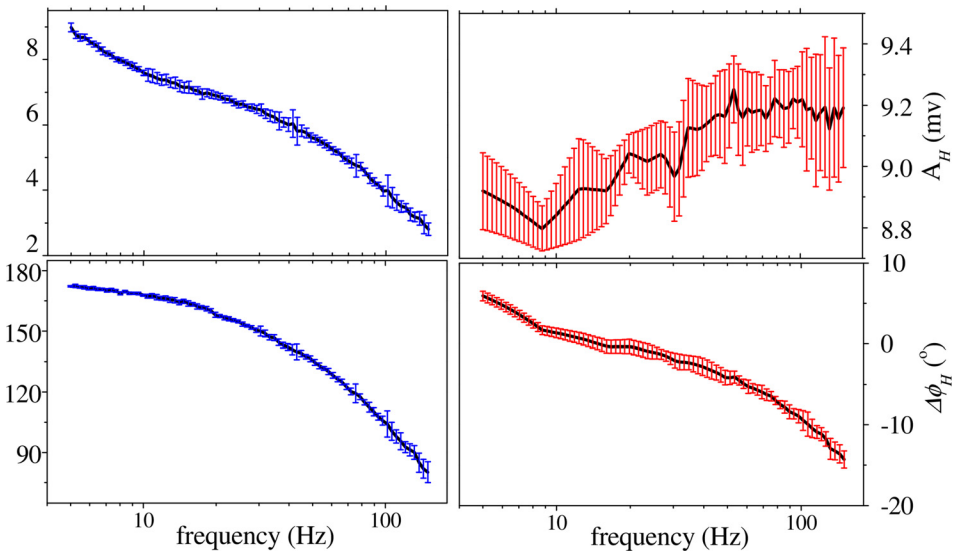

FIG. 5. Frequency dependence of the amplitude (top) and phase (bottom) signal of the photothermally modulated PL (left) from 5 Hz to 150 Hz, and detection system response (right) of the experimental setup as determined from the reflected pump light oscillations.

with $\begin{bmatrix} A & B \\ C & D \end{bmatrix} = M_1M_2M_3$, and $\begin{bmatrix} a & b \\ c & d \end{bmatrix} = M_1$.

We also assume (ii) absence of the heat convection and radiation at the top ($z = 0$) and bottom surface ($z = z_3$). This is easily satisfied due to the thermal effusivities of the involved solids being much larger than that of air,[36,37] namely, $\Phi_1|_{z=0} = \Phi_3|_{z=z3} = 0$; therefore, temperature at the top surface ($z = 0$) is achieved by

$$\Theta_0 = \Theta_1|_{z=0} = \frac{I}{2}\left(\frac{Ad}{C} - b\right). \tag{15}$$

The temperature at the top surface of the absorber layer can also be obtained by substituting Eq. (15) back to Eq. (9)

$$\Theta|_{z=l_1} = \frac{d}{ad - bc}\Theta_0 = \frac{I}{2}\frac{Ad - bC}{ad - bc}\frac{d}{C}. \tag{16}$$

Analogously, one can obtain temperature and heat flux at other interfaces, with which the coefficients E_i, F_i ($i = 1, 2, 3$) in the general solution for each layer can be obtained as well, with Eqs. (6)–(8) thus leading to the solution of temperatures at any depth (z). It is worth noting that the heat flux at the front ($\Phi_1|_{z=0}$) and rear surface ($\Phi_3|_{z=z3}$) is no longer zero if the heat loss is present. However, this can be taken into account by heat transfer coefficients as a result of radiation and/or convection, as done in Refs. 30 and 36.

IV. EXPERIMENTAL RESULTS

Fig. 5 shows the amplitude (top plot) and phase (bottom plot) of the periodically modulated PL signals, versus the modulation frequency, which was varied in logarithmic steps from 5 Hz to 150 Hz. The error bars represent the standard deviation based on 5 measurements at each frequency. Also, the system response of the setup, $H(f)$, which is mainly reflecting the frequency dependence of the electronic response of the amplifier and pump laser intensity modulation electronics, was determined, by detecting the intensity variations of the reflected pump light instead of the PL light. Since the system response (right, Fig. 5) is not flat, PL data were normalized by amplitude division and phase subtraction of $H(f)$. In addition, 180 degrees was subtracted from the normalized phase signal, in order to compensate for the sign difference between the PL signal oscillation and the temperature oscillation in Eq. (2).

Fig. 6 depicts the frequency dependent photothermal response of the sample and the best fit by using Eq. (15), with parameters summarized in Table I. The thermal properties of the three layers were taken from literature and are listed in Table I. The thicknesses of the QDs-PS layer and of the paint layer were used as fitting parameters. As shown in the last column of the Table I, the best fitting values, $12.3 \pm 0.1\ \mu$m and $26.6 \pm 0.1\ \mu$m, respectively, are in good agreement with the values measured by a micrometer. The

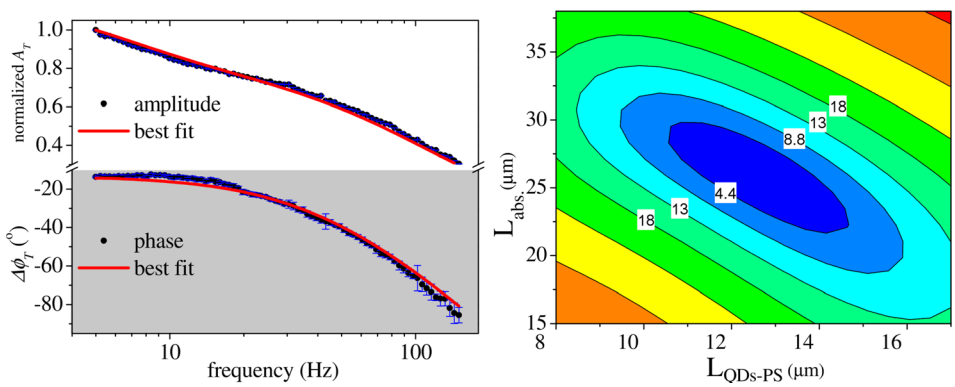

FIG. 6. Normalized photothermal response (left) of the sample in the frequency domain (dots) and best fit (solid line). The contour plot (right) of normalized χ^2-error (dB) of two fitting parameters LQDs-PS ($12.3 \pm 0.1\ \mu$m) and $L_{abs.}$ ($26.6 \pm 0.1\ \mu$m) infers a satisfactory fitting.

Reuse of AIP Publishing content is subject to the terms at: https://publishing.aip.org/authors/rights-and-permissions. Download to IP: 134.58.253.30 On: Mon, 24 Oct 2016 12:54:18

TABLE I. Fitting parameters used in Fig. 6.

	Materials	Thermal conductivity (W^{-1} m^{-1} K^{-1})	Thermal diffusivity (m^2 s^{-1})	Best-fit thickness	Thickness Nikon DIGIMICRO
Top layer	QDs-PS[38]	0.10	9.8×10^{-8}	12.3 ± 0.1 μm	13.1 μm
Middle layer	Paint[39]	1.45	2.1×10^{-7}	26.6 ± 0.1 μm	27.3 μm
Substrate layer	Red brass[40]	60.6	1.8×10^{-5}		2.05 mm

contour plot presents the dependence of the normalized sum of squared fitting errors on the two fitting parameters. The sharp minimum validates the feasibility of the proposed technique to perform photothermal characterization of the solid samples.

As a cross validation of the feasibility of the method for thermal characterization of materials, in Fig. 7, the thicknesses measured by micrometer were utilized as known parameters to fit the thermal conductivity of the top two layers. During the fit, the volumetric heat capacity (ρC_p) values of the top two layers were fixed at 1.0×10^7 J K^{-1} m^{-3}, and 6.9×10^6 J K^{-1} m^{-3} for top layer and middle layer, respectively, as calculated from Table I, while the thermal diffusivity was adapted through $\alpha = \kappa/(\rho C_p)$. As shown in Fig. 8, the experimental data (left) were again fitted well by the 1D thermal wave model, and the best fitting thermal conductivity values, 0.12 ± 0.02 W m^{-1} K^{-1}, and 1.3 ± 0.1 W m^{-1} K^{-1}, respectively, are consistent with values from literature.[35,36] This confirms the potential application of the proposed approach in the field of material evaluation, as a tool for remote thermal property determination.

The satisfactory fitting in Fig. 6 infers that the surface temperature field is a strong function of the thickness of the top layer (sensing layer), as well as of the absorber layer in the frequency range from 10 to 1000 Hz; thus, knowledge of the thickness of both the sensing and absorber layer is a prerequisite in order for an accurate reconstruction of thermal properties (Fig. 7), which this work is targeting at. By increasing the doping of QDs to ensure sufficient photoluminescence for detection, the thickness of QDs-PS layer could be decreased down to submicron scale,[7,41] which would of benefit to decrease the influence of the active layer (sensing layer) on the signals. This is illustrated in Fig. 8. The thickness of QDs-PS layer was reduced from 10 μm to 500 nm (marked by arrows), while the thickness of the absorber layer was fixed at 20 μm (left), and 500 nm (right), respectively. In

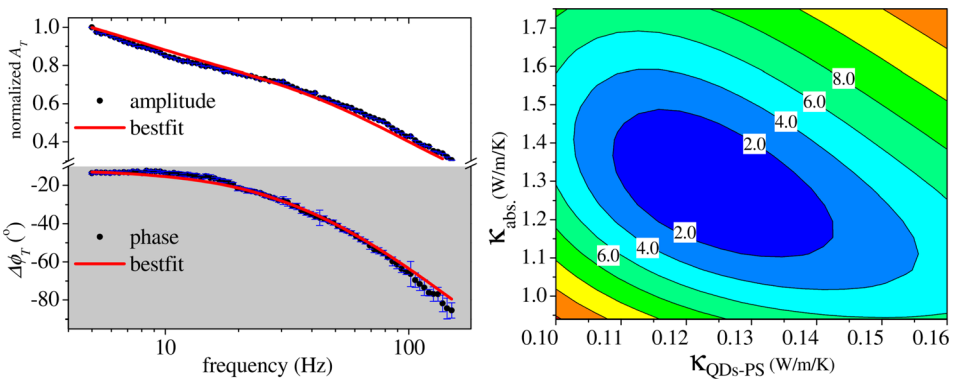

FIG. 7. Cross validation of the fitting by using micrometer-measured thicknesses as known parameters to fit the thermal conductivity of the top two layers. The best fitting values, 0.12 ± 0.02 W m^{-1} K^{-1}, and 1.3 ± 0.1 W m^{-1} K^{-1}, are in line with the values from literatures listed in Table I.

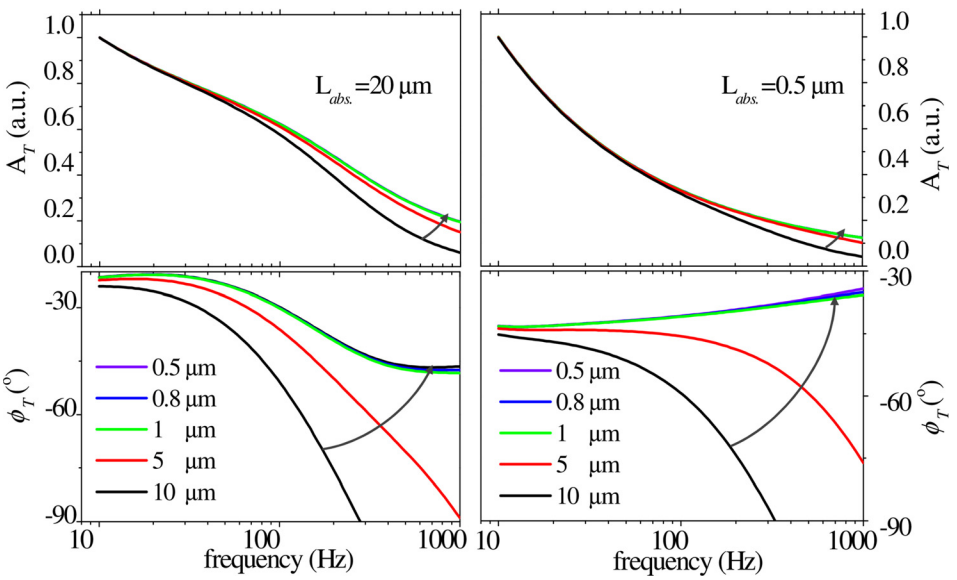

FIG. 8. The surface temperature field calculated with reduced QDs-PS layer thickness, while the thickness of the absorber layer is fixed at 20 μm (left), and 500 nm (right), respectively.

Reuse of AIP Publishing content is subject to the terms at: https://publishing.aip.org/authors/rights-and-permissions. Download to IP: 134.58.253.30 On: Mon, 24 Oct 2016 12:54:18

this simulation, the thermal wave field at the top surface of the sample was calculated by Eq. (15), with the parameters in Table I. Fig. 8 clearly shows that as the thickness of the activating layer is reduced down to 500 nm, its influence on the surface temperature field is suppressed significantly in the frequency range between 10 and 1000 Hz.

V. CONCLUSION

A photoluminescent film that consists of a temperature sensitive CdSe/ZnS–PS composite layer on the top of an optically opaque absorber layer is shown to enable simultaneous generation and detection of thermal waves, by taking advantage of the linear and fast response of the PL integration intensity of CdSe/ZnS QDs to the temperature near ambient condition between 30 and 60 °C. A specific thermal wave model was derived as well with respect to the actual sample structure and beam configuration by means of thermal quadrupole method. As a proof of concept, the amplitude and phase of the photothermally induced temperature oscillation at the sample surface were detected by a lock-in amplifier at different frequencies between 5 Hz and 150 Hz, and fitted well by the presented 1D multilayer thermal wave model. On one hand, the best fit thickness of the QDs-PS matrix layer and the absorber layer are consistent with values measured by a micrometer. On the other hand, the thermal conductivity of the top two layers, extracted from a cross-validation fitting where the thicknesses measured by micrometer were utilized as known parameters, are also in good agreement with literature values, which confirms again the potential application of the reported technique for remote thermal property characterization, thickness measurement, and the detection of flaws, such as bad thermal contact, or changes of microstructure that affect the heat transport. The reported approach can be extended to 2D lock-in thermography by implementing either an X-Y scanning of the sample, or by a CCD camera configuration in real time or stroboscopic illumination mode, to record full-field PL images of the sample surface, from which an absolute temperature image with optical resolution can be extracted on the basis of a temperature calibration process, i.e., neural network recognition of the PL intensity at each pixel.

ACKNOWLEDGMENTS

This work was financially supported by FWO, Belgium (Research Project Nos. G.0492.10 and 1.5.212.08) and KU Leuven, Belgium (Research Project No. OT/11/064). The authors would like to thank Shengping Mao for the sample thickness determination. Liwang Liu and Kuo Zhong acknowledge the support of the Chinese Scholarship Council (CSC).

[1]S. Coe, W.-K. Woo, M. Bawendi, and V. Bulović, "Electroluminescence from single monolayers of nanocrystals in molecular organic devices," Nature **420**(6917), 800–803 (2002).
[2]Q. Sun, Y. A. Wang, L. S. Li, D. Wang, T. Zhu, J. Xu, C. Yang, and Y. Li, "Bright, multicoloured light-emitting diodes based on quantum dots," Nat. Photonics **1**(12), 717–722 (2007).
[3]T.-H. Kim, K.-S. Cho, E. K. Lee, S. J. Lee, J. Chae, J. W. Kim, D. H. Kim, J.-Y. Kwon, G. Amaratunga, and S. Y. Lee, "Full-colour quantum dot displays fabricated by transfer printing," Nat. Photonics **5**(3), 176–182 (2011).
[4]V. Wood, M. J. Panzer, J. Chen, M. S. Bradley, J. E. Halpert, M. G. Bawendi, and V. Bulovic, "Inkjet-printed quantum dot-polymer composites for full-color AC-driven displays," Adv. Mater. **21**(21), 2151–2155 (2009).
[5]P. V. Kamat, "Quantum dot solar cells. The next big thing in photovoltaics," J. Phys. Chem. Lett. **4**(6), 908–918 (2013).
[6]E. H. Sargent, "Colloidal quantum dot solar cells," Nat. Photonics **6**(3), 133–135 (2012).
[7]I. L. Medintz, H. T. Uyeda, E. R. Goldman, and H. Mattoussi, "Quantum dot bioconjugates for imaging, labelling and sensing," Nat. Mater. **4**(6), 435–446 (2005).
[8]J. K. Jaiswal and S. M. Simon, "Potentials and pitfalls of fluorescent quantum dots for biological imaging," Trends Cell Biol. **14**(9), 497–504 (2004).
[9]C. J. Murphy, "Peer reviewed: Optical sensing with quantum dots," Anal. Chem. **74**(19), 520 A–526 A (2002).
[10]P. Jing, J. Zheng, M. Ikezawa, X. Liu, S. Lv, X. Kong, J. Zhao, and Y. Masumoto, "Temperature-dependent photoluminescence of CdSe-core CdS/CdZnS/ZnS-multishell quantum dots," J. Phys. Chem. C **113**(31), 13545–13550 (2009).
[11]G. W. Walker, V. C. Sundar, C. M. Rudzinski, A. W. Wun, M. G. Bawendi, and D. G. Nocera, "Quantum-dot optical temperature probes," Appl. Phys. Lett. **83**(17), 3555–3557 (2003).
[12]S. Li, K. Zhang, J.-M. Yang, L. Lin, and H. Yang, "Single quantum dots as local temperature markers," Nano Lett. **7**(10), 3102–3105 (2007).
[13]O. Labeau, P. Tamarat, and B. Lounis, "Temperature dependence of the luminescence lifetime of single CdSe/ZnS quantum dots," Phys. Rev. Lett. **90**(25), 257404 (2003).
[14]D. Jaque and F. Vetrone, "Luminescence nanothermometry," Nanoscale **4**(15), 4301–4326 (2012).
[15]L. Liu, S. Creten, Y. Firdaus, J. J. A. F. Cuautle, M. Kouyaté, M. Van der Auweraer, and C. Glorieux, "Fluorescence spectra shape based dynamic thermometry," Appl. Phys. Lett. **104**(3), 031902 (2014).
[16]T. Munro, L. Liu, C. Glorieux, and H. Ban, "CdSe/ZnS quantum dot fluorescence spectra shape-based thermometry via neural network reconstruction," J. Appl. Phys. **119**, 214903 (2016).
[17]X.-D. Wang, O. S. Wolfbeis, and R. J. Meier, "Luminescent probes and sensors for temperature," Chem. Soc. Rev. **42**(19), 7834–7869 (2013).
[18]L. Aigouy, B. Samson, G. Julié, V. Mathet, N. Lequeux, C. N. Allen, H. Diaf, and B. Dubertret, "Scanning near-field optical microscope working with a CdSe/ZnS quantum dot based optical detector," Rev. Sci. Instrum. **77**(6), 063702 (2006).
[19]A. Cadiau, C. D. Brites, P. M. Costa, R. A. Ferreira, J. Rocha, and L. D. Carlos, "Ratiometric nanothermometer based on an emissive Ln3+organic framework," ACS Nano **7**(8), 7213–7218 (2013).
[20]L. M. Maestro, E. M. Rodríguez, F. S. Rodríguez, M. I.-D. la Cruz, A. Juarranz, R. Naccache, F. Vetrone, D. Jaque, J. A. Capobianco, and J. G. Solé, "CdSe quantum dots for two-photon fluorescence thermal imaging," Nano Lett. **10**(12), 5109–5115 (2010).
[21]L. Liu, K. Zhong, T. Munro, S. Alvarado, R. Côte, S. Creten, E. Fron, H. Ban, M. Van der Auweraer, and N. Roozen, "Wideband fluorescence-based thermometry by neural network recognition: Photothermal application with 10 ns time resolution," J. Appl. Phys. **118**(18), 184906 (2015).
[22]D. Valerini, A. Creti, M. Lomascolo, L. Manna, R. Cingolani, and M. Anni, "Temperature dependence of the photoluminescence properties of colloidal Cd Se/Zn S core/shell quantum dots embedded in a polystyrene matrix," Phys. Rev. B **71**(23), 235409 (2005).
[23]W. G. van Sark, P. L. Frederix, A. A. Bol, H. C. Gerritsen, and A. Meijerink, "Blueing, bleaching, and blinking of single CdSe/ZnS quantum dots," ChemPhysChem **3**(10), 871–879 (2002).
[24]A. Joshi, K. Narsingi, M. Manasreh, E. Davis, and B. Weaver, "Temperature dependence of the band gap of colloidal CdSe/ZnS core/shell nanocrystals embedded into an ultraviolet curable resin," Appl. Phys. Lett. **89**(13), 131907 (2006).
[25]S. N. Kuznetsov, A. B. Cheremisin, and G. B. Stefanovich, "Photoluminescence response of colloidal quantum dots on VO2 film across metal to insulator transition," Nanoscale Res. Lett. **9**(1), 612 (2014).
[26]S. Wang, S. Westcott, and W. Chen, "Nanoparticle luminescence thermometry," J. Phys. Chem. B **106**(43), 11203–11209 (2002).
[27]B. Han, W. L. Hanson, K. Bensalah, A. Tuncel, J. M. Stern, and J. A. Cadeddu, "Development of quantum dot-mediated fluorescence thermometry for thermal therapies," Ann. Biom. Eng. **37**(6), 1230–1239 (2009).

Reuse of AIP Publishing content is subject to the terms at: https://publishing.aip.org/authors/rights-and-permissions. Download to IP: 134.58.253.30 On: Mon, 24 Oct 2016 12:54:18

[28]S. Bialkowski, *Photothermal Spectroscopy Methods for Chemical Analysis* (John Wiley & Sons, 1996), Vol. 134.
[29]L. Liu, C. Wang, X. Yuan, and A. Mandelis, "Similarity normalization method for thermal conductivity depth profile reconstructions from inhomogeneous cylindrical and flat solids using thermal waves," J. Appl. Phys. **107**(5), 053503 (2010).
[30]A. Salazar, R. Fuente, E. Apinaniz, A. Mendioroz, and R. Celorrio, "Simultaneous measurement of thermal diffusivity and optical absorption coefficient using photothermal radiometry. II Multilayered solids," J. Appl. Phys. **110**(3), 033516 (2011).
[31]A. C. Balazs, T. Emrick, and T. P. Russell, "Nanoparticle polymer composites: where two small worlds meet," Science **314**(5802), 1107–1110 (2006).
[32]M. A. Hines and P. Guyot-Sionnest, "Synthesis and characterization of strongly luminescing ZnS-capped CdSe nanocrystals," J. Phys. Chem. **100**(2), 468–471 (1996).
[33]J. Wan, J. Brebner, R. Leonelli, G. Zhao, and J. Graham, "Temperature dependence of free-exciton photoluminescence in crystalline GaTe," Phys. Rev. B **48**(8), 5197 (1993).
[34]Y. Varshni, "Temperature dependence of the energy gap in semiconductors," Physica **34**(1), 149–154 (1967).
[35]O. Madelung, *Numerical Data and Functional Relationships in Science and Technology*, Crystal and Solid State Physics, Semiconductors: Special Systems and Topics, Comprehensive Index for III/17a··· i (Springer-Verlag, 1985).
[36]K. Martínez, E. Marín, C. Glorieux, A. Lara-Bernal, A. Calderón, G. P. Rodríguez, and R. Ivanov, "Thermal diffusivity measurements in solids by photothermal infrared radiometry: Influence of convection–radiation heat losses," Int. J. Thermal Sci. **98**, 202–207 (2015).
[37]J. Ordonez-Miranda and J. Alvarado-Gil, "Thermal quadrupole method applied to flat and spherical semi-transparent multilayers heated up with a modulated laser beam," J. Appl. Phys. **112**(11), 114902 (2012).
[38]J. E. Mark, *Physical Properties of Polymers Handbook* (Springer, 1996).
[39]O. Raghu and J. Philip, "Thermal properties of paint coatings on different backings using a scanning photo acoustic technique," Meas. Sci. Technol. **17**(11), 2945 (2006).
[40]C. Kothandaraman, *Heat and Mass Transfer Data Book* (New Age International, 2004).
[41]B. Suo, X. Su, J. Wu, D. Chen, A. Wang, and Z. Guo, "Poly (vinyl alcohol) thin film filled with CdSe–ZnS quantum dots: Fabrication, characterization and optical properties," Mater. Chem. Phys. **119**(1), 237–242 (2010).

Reuse of AIP Publishing content is subject to the terms at: https://publishing.aip.org/authors/rights-and-permissions. Download to IP: 134.58.253.30 On: Mon, 24 Oct 2016 12:54:18